





Cite this: *Nanoscale*, 2022, **14**, 6449

## Rational design of engineered H-ferritin nanoparticles with improved siRNA delivery efficacy across an *in vitro* model of the mouse BBB†

Ziwei Yuan,<sup>a</sup> Bin Wang,<sup>a</sup> Yilong Teng,<sup>a</sup> William Ho,<sup>b</sup> Bin Hu,<sup>a</sup> Kofi Oti Boakye-Yiadam,<sup>a</sup> Xiaoyang Xu \*<sup>b</sup> and Xue-Qing Zhang \*<sup>a</sup>

Gene therapy holds tremendous potential for the treatment of incurable brain diseases including Alzheimer's disease (AD), stroke, glioma, and Parkinson's disease. The main challenge is the lack of effective gene delivery systems traversing the blood–brain barrier (BBB), due to the complex microvessels present in the brain which restrict substances from the circulating blood passing through. Recently, increasing efforts have been made to develop promising gene carriers for brain-related disease therapies. One such development is the self-assembled heavy chain ferritin (HF<sub>n</sub>) nanoparticles (NPs). HF<sub>n</sub> NPs have a unique hollow spherical structure that can encapsulate nucleic acid drugs (NADs) and specifically bind to cancer cells and BBB endothelial cells (BBB ECs) *via* interactions with the transferrin receptor 1 (TFR1) overexpressed on their surfaces, which increases uptake through the BBB. However, the gene-loading capacity of HF<sub>n</sub> is restricted by its limited interior volume and negatively charged inner surface; therefore, these drawbacks have prompted the demand for strategies to remould the structure of HF<sub>n</sub>. In this work, we analyzed the three-dimensional (3D) structure of HF<sub>n</sub> using Chimera software (v 1.14) and developed a class of internally cationic HF<sub>n</sub> variants (HF<sub>n</sub><sup>+</sup> NPs) through arginine mutation on the luminal surface of HF<sub>n</sub>. These HF<sub>n</sub><sup>+</sup> NPs presented powerful electrostatic forces in their cavities, and exhibited higher gene encapsulation efficacy than naive HF<sub>n</sub>. The top-performing candidate, HF<sub>n</sub>2, effectively delivered siRNA to glioma cells after traversing the BBB and achieved the highest silencing efficacy among HF<sub>n</sub><sup>+</sup> NPs. Overall, our findings demonstrate that HF<sub>n</sub><sup>+</sup> NPs obtained by this genetic engineering method provide critical insights into the future development of nucleic acid delivery carriers with BBB-crossing ability.

Received 30th November 2021.  
Accepted 28th March 2022

DOI: 10.1039/d1nr07880a

[rsc.li/nanoscale](http://rsc.li/nanoscale)

### 1. Introduction

The blood–brain barrier (BBB) is a highly structured network of microvessels composed of microvascular endothelial cells with the support of pericytes and astrocytes, maintaining brain homeostasis through selective permeability.<sup>1,2</sup> In serving this purpose, the dense endothelial structure, significant transendothelial electrical resistance (TEER) and efflux pumps restrict the transport of a majority of exogenous small therapeutic molecules and macromolecules.<sup>3,4</sup> Therefore, drug delivery to the brain has long posed severe challenges to

researchers, and efficient therapeutics need to be urgently developed, as brain diseases are critical and often fatal events.<sup>5</sup> Gene therapy, including small RNAs (*e.g.*, siRNA, mRNA, and miRNA), has long been a research focus due to its remarkable therapeutic effect in virtually any disease.<sup>6</sup> Recently, it has shed new light on the treatment of incurable brain disorders, such as glioblastoma multiforme (GBM).<sup>7</sup> However, since nucleic acid drugs (NADs) are unstable and negatively charged, they tend to be degraded under physiological conditions and have weak cellular internalization, which leads to low transfection efficiency *in vivo*.<sup>8</sup> Hence, there exists a tremendous demand for the development of appropriate delivery vehicles to protect nucleic acids and improve their delivery efficiency across the BBB.<sup>9,10</sup>

Various developments in generic gene delivery have been reported involving carriers such as adeno-associated viruses (AAVs), lipid nanoparticles (LNPs), cationic polymers, and inorganic nanoparticles (NPs), but there have been few advances in gene delivery across the specialized BBB. Recently,

<sup>a</sup>Engineering Research Center of Cell & Therapeutic Antibody, Ministry of Education, and School of Pharmacy, Shanghai Jiao Tong University, 800 Dongchuan Road, Shanghai 200240, PR China. E-mail: [xueqingzhang@sjtu.edu.cn](mailto:xueqingzhang@sjtu.edu.cn)

<sup>b</sup>Department of Chemical and Materials Engineering, New Jersey Institute of Technology, Newark, NJ, 07102, USA. E-mail: [xiaoyang@njit.edu](mailto:xiaoyang@njit.edu)

† Electronic supplementary information (ESI) available. See DOI: <https://doi.org/10.1039/d1nr07880a>

Deverman *et al.* explored AAV variants for efficient gene delivery to the mouse brain. However, these capsids seemed to be species specific and their potency for gene therapy needs to be further studied.<sup>11,12</sup> Protein NPs are emerging as a potential solution due to their high biocompatibility and unique features which depend on the particular protein.<sup>13–15</sup> In particular, heavy chain ferritin (HF<sub>n</sub>), can bind specifically to transferrin receptor 1 (TfR1), one of the major receptors expressed on human or rodent BBB endothelial cells (BBB ECs) and cancer cells,<sup>16</sup> making it a promising biological platform for which to build a carrier to traverse the BBB.<sup>8,17</sup> Due to its inner cavity being 8 nm in diameter,<sup>18</sup> HF<sub>n</sub> is capable of loading nucleic acids and protecting them from degradation.<sup>19</sup> In addition, HF<sub>n</sub> possesses a unique pH-mediated biophysical property of self-assembly–disassembly, which contributes to structural stability under neutral physiological conditions and the release of nucleic acids in an acidic intracellular endosome environment.<sup>20,21</sup>

Naive HF<sub>n</sub> has a potent capacity for storing metal ions but not nucleic acids due to its negatively charged interior surface.<sup>22–25</sup> Although nucleic acids can be encapsulated in the cavity of unmodified ferritin,<sup>17</sup> the encapsulation efficiency (EE) remains a hurdle. The entrapment of negatively charged nucleic acids depends mainly on the electrostatic interaction between genes and carriers,<sup>26</sup> and nucleic acids hardly bind to the negatively charged internal surface of HF<sub>n</sub> NPs.<sup>27</sup> The poor gene-loading capacity has become a significant limitation in the applications of HF<sub>n</sub>.<sup>28,29</sup> Despite extensive efforts to encapsulate cargo molecules in HF<sub>n</sub>, such as pH-mediated disassembly and reassembly,<sup>30</sup> denaturing buffer loading strategy<sup>31</sup> and Ca<sup>2+</sup>-participating self-assembly,<sup>32</sup> effective enhancement of the EE is still elusive. Additionally, multiple functional motifs have been modified on the external surface of HF<sub>n</sub> *via* various chemical or genetic methods, but few attempts have been made to remould the cavity itself.<sup>18,33</sup>

In this work, we rationally designed a class of *de novo* internally cationic HF<sub>n</sub> variants (HF<sub>n</sub><sup>+</sup> NPs) and predicted their three-dimensional (3D) structures and physicochemical properties using Chimera software. Previous studies demonstrated that electrostatic binding interactions provided a strong driving force for the formation of host–guest complexes,<sup>34,35</sup> and genetic engineering methods could readily introduce additional functionalities to proteins.<sup>36</sup> By introducing arginine mutations on the luminal surface of HF<sub>n</sub> through genetic manipulation, we altered the internal surface conformation and the amount of positive charge within HF<sub>n</sub> NPs. We modulated the negative charges on the inner surface of HF<sub>n</sub> into positive charges, thereby assisting siRNA encapsulation during NP formation to enhance the EE of HF<sub>n</sub> NPs.<sup>37,38</sup> Considering the limited cavity size of HF<sub>n</sub>, siRNAs, relatively small-sized RNA molecules, were chosen as the cargo molecule. This natural protein that innately traffics through the BBB was successfully transformed into a vehicle for efficient nucleic acid delivery to the brain while preserving its stability, assembly capacity, and bioactivity. Under acidic conditions (pH < 3), HF<sub>n</sub><sup>+</sup> was broken down into subunits and incubated

with siRNA to achieve adsorption. After incubation, the pH was adjusted to 7.4 to facilitate the reformation of nanostructures and siRNA was loaded into the cavity of the reconstituted HF<sub>n</sub><sup>+</sup> NPs (Scheme 1A). Moreover, HF<sub>n</sub><sup>+</sup> could traverse the BBB ECs through TfR1-mediated transcytosis and efficiently knock down the expression of target mRNA in GBM cells through TfR1-mediated endocytosis (Scheme 1B), thus showing promise in silencing genes related to brain tumor progression by RNAi (Scheme 1C). Overall, these redesigned HF<sub>n</sub><sup>+</sup> variants will provide an insight into the rational *de novo* design of versatile protein cages for BBB traversal and effective gene delivery.

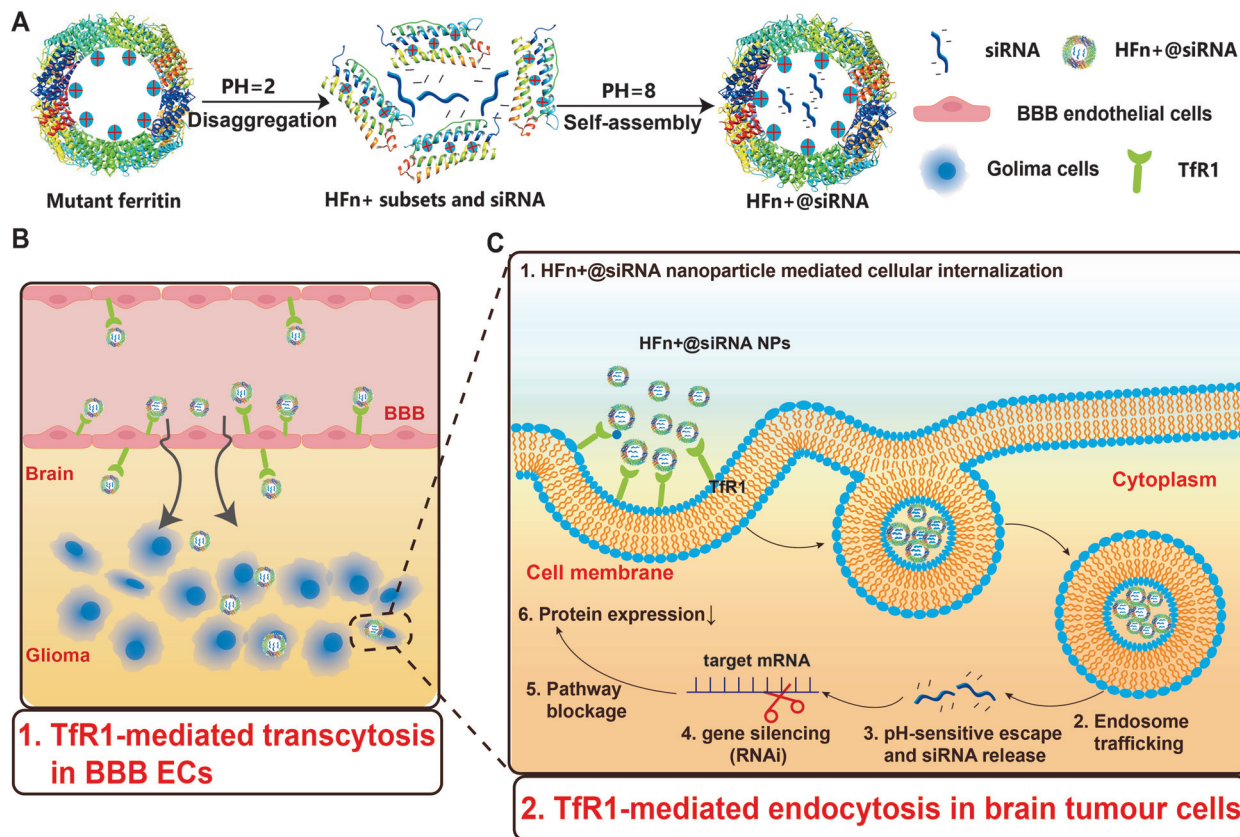
## 2. Materials and methods

### 2.1. Materials

Plasmid pET-30a (+) was purchased from Hunan Fenghui Biotechnology Co. Ltd (China). The hFTH gene (HG13217-G) was obtained as a cDNA clone from Sino Biological Inc. (China). FITC and isopropyl-β-D-thiogalactopyranoside (IPTG) were purchased from Sigma-Aldrich Co. Ltd (USA). Kanamycin, ammonium sulfate and gelatin were purchased from Shanghai Aladdin Bio-Chem Technology Co. Ltd (China). Dulbecco's modified Eagle's medium (DMEM), fetal bovine serum (FBS), trypsin-EDTA, and penicillin–streptomycin solution were purchased from Gibco (USA). Akata start (GE, USA) was used to purify the target proteins. siLuc was synthesized by Suzhou Beixin Biotechnology Co. Ltd (China). Cy5-labeled siRNA was purchased from Shanghai Jima Pharmaceutical Technology Co. Ltd (China). Rabbit anti-claudin 5 antibody (bs-1241R) and mouse anti-CD31 antibody (BH0190) were purchased from Beijing Biosynthesis Biotechnology Co. Ltd (China). LysoTracker Green (C1047S), DAPI (C1002), and the Mycoplasma PCR Detection Kit (C0301S) were purchased from Beyotime (Shanghai, China). Other reagents were purchased from Sigma-Aldrich (USA) unless otherwise indicated.

### 2.2. General cell culture

A HeLa cell line stably expressing both reporter proteins – firefly *Photinus pyralis* and *Renilla reniformis* luciferase (Dual-Luc HeLa)<sup>39</sup> – was obtained from Alnylam Pharmaceuticals, Inc. and was cultured in DMEM containing 10% FBS and 600 μg mL<sup>-1</sup> puromycin. Bioluminescent mouse glial cell lines correlated to glioblastoma (Luc-GL261 cells) and immortalized mouse cerebrovascular ECs line (bEnd.3 cells) were obtained from the American Type Culture Collection (ATCC). Luc-GL261 cells were engineered to stably express firefly luciferase alone and were cultured in DMEM containing 10% FBS and 1200 μg mL<sup>-1</sup> G418 disulfate salt, while bEnd.3 cells were cultured in DMEM containing 10% FBS. All cells used in the study were between passage numbers 3 and 6. The doubling time of cell cultures was estimated from the population size and generally was about 48 h for cell lines and 72 h for primary cells. All cell cultures used in this work were free of mycoplasma contamination as determined using the Mycoplasma PCR Detection Kit (Fig. S1†).



**Scheme 1** Schematic illustration of HFN+ NPs-mediated siRNA delivery for regulating brain tumor progression. (A) 3D model of the HFN+ subunit and self-assembled HFN+ NPs, generated using Chimera simulation software. These HFN+ NPs encapsulated siRNA using an assembly/disassembly method. (B) The siRNA@HFN+ NPs traverse the BBB through Tfr1-mediated transcytosis and target glioma cells via Tfr1-mediated endocytosis. (C) Following the cellular uptake of siRNA@HFN+ NPs, siRNA released from the endosomes interferes with protein expression levels via RNAi and has the potential to block brain cancer-related pathways for disease therapy.

### 2.3. Construction of HFN+ expression plasmids

A series of primers containing arginine mutation sites were biosynthesized, and the sequence information is detailed in Table SI.† We obtained cationic mutation fragments using primers through an arginine site-directed mutagenesis method. The HFN+ cDNAs were cloned using an overlap and extension PCR method. Each gene clone was ligated into a pET-30a (+) plasmid to yield the expression vectors, pET-HFN/HFN+. The constructed vectors were subsequently transformed into *E. coli* BL21(DE3), and transformants were obtained by kanamycin-resistance selection.

### 2.4. Biosynthesis of HFN and HFN+ NPs

Briefly, the expression vectors pET-HFN and pET-HFN+ were transformed into *E. coli* BL21(DE3) according to the manufacturer's instructions. A 1 L LB-kanamycin (50 mg L<sup>-1</sup>) culture of both *E. coli* BL21(DE3)/HFN and *E. coli* BL21(DE3)/HFN+ was grown at 37 °C until the OD<sub>600</sub> reached 0.6–1.0, then induced with 1 mM IPTG and further incubated at 37 °C for 12 h. After incubation, *E. coli* cells were harvested by centrifugation at 5000g for 45 min and the pellets were resuspended in phosphate-buffered saline (PBS) buffer (50 mM PO<sub>4</sub><sup>3-</sup>, 0.15 M NaCl,

pH 7.4). Both HFN and HFN+ proteins were lysed by high-pressure homogenization and sonication until the cell lysates were clear, following the centrifugation of lysates at 10 000g for 30 min. After removing cell debris, their supernatants were heated at 65 °C for 20 min and the resulting supernatants of HFN and HFN+ were stored at –20 °C until purification.

### 2.5. Western blotting (WB) analysis

The supernatants of HFN+ lysates after heating were isolated to measure the protein concentration via a bicinchoninic acid (BCA) protein assay kit. The supernatants containing 20 μg of protein were loaded onto a 12% SDS-polyacrylamide gel electrophoresis (SDS-PAGE) at 120 V to perform immunoblotting and then transferred to polyvinylidene fluoride (PVDF) membranes using a standard method. The membranes were blocked using a solution of 5% bovine serum albumin (BSA) in Tris buffer with tween-20 (TBST) for 2 h and incubated with the corresponding primary antibodies overnight at 4 °C. After that, the membranes were incubated with HRP-linked second antibodies (1:500) (Proteintech, USA) at room temperature (RT) for 1 h. Pierce ECL WB substrate was used to observe the signals.

## 2.6. Purification of HF<sub>n</sub> and HF<sub>n</sub>+ NPs

For HF<sub>n</sub>, the resulting supernatant was precipitated using ammonium sulfate (520 g L<sup>-1</sup>) and the precipitate was collected *via* centrifugation at 22 000g for 45 min. Then it was dissolved in PBS buffer. After dialyzing out the ammonium sulfate, DNase I and RNase A (Sigma Aldrich) were added to final concentrations of 60 μg mL<sup>-1</sup> and 100 μg mL<sup>-1</sup>, respectively, and incubated for 30 min at 37 °C. The resulting supernatant was purified *via* size exclusion chromatography (SEC) on a Superdex 200 PG XK 16/100 column (GE Healthcare, USA). The typical yield of HF<sub>n</sub> was 300 mg per 1 L patch.

As HF<sub>n</sub>+ with His-tag were capable of loading endogenous RNA molecules during their expression in *E. coli*, optimized protocols were developed to isolate the empty cage with good purity. These involved using a high ionic strength buffer to weaken the interaction with nucleic acids and extended incubation with DNase I and RNase A. Each cell pellet from 1 L of culture was resuspended in 50 mL of lysis buffer (50 mM PO<sub>4</sub><sup>3-</sup>, 0.15 M NaCl, pH 7.4) supplemented with lysozyme (1 mg mL<sup>-1</sup>), DNase I (10 U mL<sup>-1</sup>), RNase A (5 U mL<sup>-1</sup>), and protease inhibitor cocktail (Sigma). Then the lysates were incubated at 37 °C for 1 h. After lysis comprising high-pressure homogenization, sonication, thermal treatment, and centrifugation (10 000g) for 30 min, the supernatant was loaded onto the HisTrap™ HP column (GE Healthcare, USA). The column was washed with a stepwise imidazole gradient to remove the contaminants and then the target protein was eluted with elution buffer (50 mM PBS, 0.15 M NaCl, 500 mM imidazole, pH 7.4). Purified HF<sub>n</sub>2 and HF<sub>n</sub>4 in the different imidazole concentrations of elution buffers were determined qualitatively *via* WB analysis. After the primary purification, they were incubated for 0.5 h at 37 °C to digest any contaminant *E. coli* RNA, which was not removed during the HisTrap™ column purification. The proteins were then ready for SEC and the final purified product was collected and washed several times with the PBS storage buffer using an Amicon filter (MWCO = 100 kDa, Millipore). Like before, the final productivity of HF<sub>n</sub>+ was measured using the BCA protein assay kit. It should be noted that all storage of the proteins and experiments were carried out at RT unless specified otherwise.

## 2.7. Preparation and characterization of HF<sub>n</sub> and HF<sub>n</sub>+

The yielded HF<sub>n</sub> and HF<sub>n</sub>+ NPs were characterized using a transmission electron microscope (TEM, Thermo Scientific Talos, USA) for morphology analysis and dynamic light scattering (DLS, Malvern, USA) for mean particle size and zeta potential characterization. The purity of protein products was analyzed using 12% SDS-PAGE. The final protein concentrations were determined *via* UV-vis absorbance at 562 nm using the BCA protein assay kit (Beyotime). The stability of HF<sub>n</sub> and HF<sub>n</sub>+ was evaluated using native polyacrylamide gel electrophoresis (native PAGE).

## 2.8. Cy5-siRNA encapsulation in HF<sub>n</sub>+ NPs

Ferritin can break down into subunits under a certain acid or alkaline conditions and reassemble when the pH is adjusted

to physiological conditions.<sup>40–42</sup> In this study, the encapsulation of Cy5-siRNA into HF<sub>n</sub>+ was achieved *via* a pH-mediated disassembly/assembly method.<sup>32</sup> The dissociation of HF<sub>n</sub>+ into discrete subunits was achieved by lowering the pH to 2.0 with HCl. Meanwhile, Cy5-siRNA was added into the disassembled HF<sub>n</sub>+ solution, and the molar ratio of Cy5-siRNA/protein was chosen as 1 : 8 because it was reported to be the optimal molar ratio for HF<sub>n</sub> to deliver siRNA.<sup>17,28</sup> After co-incubation for 20 min, the mixture was adjusted to about pH 7.4 with NaOH and then stirred for another 2 h at room temperature. The reassembled NPs were treated with 3 mg mL<sup>-1</sup> RNase A at 37 °C for 30 min, followed by treatment with 5 mg mL<sup>-1</sup> proteinase K at 37 °C for 30 min. The unwrapped free siRNA outside of the HF<sub>n</sub>/HF<sub>n</sub>+ was digested using RNase A and proteinase K degraded the RNase A. To demonstrate the successful loading of Cy5-siRNA, 2% agarose gel electrophoresis (AGE) was carried out. The bands of Cy5-siRNA and siRNA@HF<sub>n</sub>+ NPs were visualized using an ultraviolet imager.

## 2.9. EE evaluation of the Cy5-siRNA@HF<sub>n</sub>/HF<sub>n</sub>+ NPs

To calculate the EE of siRNA@HF<sub>n</sub>/HF<sub>n</sub>+, Cy5-siRNA was used as a locator for quantitative evaluation. Cy5-siRNA@HF<sub>n</sub>/HF<sub>n</sub>+ NPs were prepared using the previous method at molar ratios of 1 : 1, 1 : 3, 1 : 5, 1 : 8, 1 : 10, and 1 : 15. The free unencapsulated siRNA was removed with an Amicon filter (MWCO = 100 kDa, Millipore). Then the pH of the NPs was adjusted to 2.0 using HCl, and the fluorescence intensity of Cy5 was detected after 15 min. The EE was calculated using the following formula: EE (%) =  $C_t/C_{total} \times 100$  (where  $C_t$  is the concentration of Cy5-siRNA released from NPs and  $C_{total}$  represents the concentration of the total added Cy5-siRNA in the NPs). Moreover, the disassembled NPs at pH 2.0 were immediately analyzed using 2% AGE and subsequently imaged.

## 2.10. RNase resistance and NP stability

The main factor hindering effective siRNA delivery *in vivo* is enzymatic degradation.<sup>43</sup> To evaluate the protective effect of HF<sub>n</sub>+ on siRNA, Cy5-siRNA@HF<sub>n</sub>/HF<sub>n</sub>+ NPs were treated with RNase A (5 μL, 3 mg mL<sup>-1</sup>) for different time intervals (0, 4, 8, 16, and 24 h) and the digestion of RNase A was aborted as before. The 2% AGE was run to verify its protection. The rest of the NPs after 24 h of RNase digestion were stored at 4 °C for 4 weeks. Then the same amount of naked siRNA (500 ng) was used as the control. To check the serum stability of NPs, samples were incubated with serum-containing medium (10% FBS, pH = 7.4) for different durations. In these experiments, the gel was run at 110 V for 20 min and subsequently imaged *via* an ultraviolet imager.

## 2.11. *In vitro* release of siRNA from the NPs

For the assessment of the release kinetics, Cy5-siRNA was encapsulated into the HF<sub>n</sub>, HF<sub>n</sub>2 and HF<sub>n</sub>4 NPs. A suspension of Cy5-siRNA@NPs in PBS at either pH 5.0 or pH 7.4 was aliquoted (500 μL) into several semipermeable minialysis tubes (molecular mass cutoff of 100 kDa; Pierce) and incubated with gentle stirring in frequently renewed PBS (pH 5.0 or pH 7.4) at 37 °C in the dark. Cumulative release of siRNA

was measured at predetermined time points. For siRNA quantification, a standard curve correlating fluorescence with Cy5-siRNA concentration was used to determine the amount of Cy5-siRNA encapsulated within the NPs. The fluorescence intensity was measured using a multimodal plate reader (excitation/emission 633/670 nm; Tecan, Switzerland).

### 2.12. Assessment of endosomal escape of Cy5-siRNA@NPs

GL261 cells were seeded into 35 mm Petri dishes at a density of  $2 \times 10^5$  cells per dish and incubated for 24 h in 1 ml of 10% FBS-containing DMEM until approximately 40–50% confluence. Cy5-siRNA@HF<sub>n</sub>, Cy5-siRNA@HF<sub>n</sub>2, and Cy5-siRNA@HF<sub>n</sub>4 NPs were then added and incubated with the cells for 2, 4, and 8 h, respectively. The medium was then removed, and the cells were rinsed three times with PBS. DAPI (Beyotime, C1002) was used to stain the nuclei, and LysoTracker Green (Beyotime, C1047S) was used to stain late endosomes. The cells were observed and imaged using a laser scanning confocal microscopy (LSCM, Leica, USA).

### 2.13. Cell viability assay

The cytotoxicity of HF<sub>n</sub> and HF<sub>n</sub>+ to HeLa, GL261, and primary microglial cells was determined using the Cell Counting Kit-8 (CCK-8) assay. Briefly, cells were seeded into a 96-well plate ( $1 \times 10^4$  cells per well) and incubated for 24 h to allow complete attachment. Then they were treated with HF<sub>n</sub> and HF<sub>n</sub>+ NPs at different concentrations. An equal volume of PBS was used for the control group. After different periods of incubation at 37 °C, the mixture was replaced with CCK-8 reagent-containing complete medium. After 4 h, absorbance at 490 nm of samples ( $OD_{\text{sample}}$ ) was measured using a multimodal plate reader (Tecan, Switzerland). The untreated cells were taken as a negative control ( $OD_{\text{control}}$ ). The medium not containing cells and samples was taken as a blank group ( $OD_{\text{blank}}$ ). The relative cell viability was calculated using the following formula: cell viability (%) =  $(OD_{\text{sample}} - OD_{\text{blank}}) / (OD_{\text{control}} - OD_{\text{blank}}) \times 100$ .

### 2.14. *In vitro* cell uptake studies

Flow cytometry was used for quantitatively investigating the cellular uptake of the Cy5-siRNA@HF<sub>n</sub>/HF<sub>n</sub>2/HF<sub>n</sub>4 NPs. Briefly, HeLa and GL261 cells were seeded into 24-well plates (Corning) at a density of  $5 \times 10^4$  cells per well for 24 h to reach 80% confluence, and the culture medium was next replaced with the medium containing 1.5 μM and 3 μM Cy5-siRNA@HF<sub>n</sub>/HF<sub>n</sub>+ NPs at a ratio of 8 : 1. Untreated cells were used as a negative control. After another 12 h, single-cell suspensions were prepared by digestion with 0.25% trypsin followed by filtration through a 300-mesh sieve. From each well, 50 000 events were recorded and analyzed immediately using a FACS Calibur flow cytometry system (BD Biosciences, USA).

### 2.15. *In vitro* siRNA transfection

We used siLuc for encapsulation at a molar ratio of siLuc/protein of 1 : 8. The samples were washed with PBS to remove the free siRNA. Dual-Luc HeLa cells were seeded into 96-well

plates ( $1 \times 10^4$  cells per well) for 24 h to reach 70–80% confluency. Cells were then transfected with 1.5 μM siLuc@HF<sub>n</sub>/HF<sub>n</sub>+ NPs overnight and replaced with the fresh medium followed by further incubation in the medium for one day. The expression of firefly and *Renilla* luciferase in HeLa cells was determined by Dual-Glo™ Luciferase assay kits. All the transfection experiments were performed in triplicate. Once we screened the optimal HF<sub>n</sub>+ variants, we used the higher dose (3.0 μM) as the transfection concentration for further research. Differently, the expression of firefly luciferase in Luc-GL261 cells was detected using the Luciferase Assay System protocol. The silencing of siLuc@HF<sub>n</sub>+ was determined by comparing the detected protein expression levels in treated groups against the untreated control and termed the relative firefly luciferase expression.

### 2.16. Immunofluorescence of bEnd.3 cells

bEnd.3 cells were seeded at a density of  $5 \times 10^4$  cells per cm<sup>2</sup> onto the upper chamber of the transwell pre-coated with gelatin (2% w:v) and allowed to grow until 70–80% confluency. Cells were fixed with 4% paraformaldehyde for 20 min, washed three times with PBS, permeabilized with 0.5% Triton X-100 in PBS for 5 min and then blocked with 3% BSA for 30 min at RT after three washes with PBS. Primary antibodies were incubated overnight at 4 °C under permeabilized conditions: mouse anti-CD31 antibody (Bioss, BH0190, 1 : 200) and rabbit anti-claudin 5 antibody (Bioss, bs-1241R, 1 : 100). The following secondary antibodies were incubated for 60 min at RT in the dark: goat anti-mouse Cy5 (Servicebio, GB27301, 1 : 400) and goat anti-rabbit AlexaFluor 488 (Servicebio, GB25303, 1 : 200). The nuclei were counterstained by incubating with DAPI (Beyotime, C1002, 5 μg μL<sup>-1</sup>) for 10 min. For imaging, laser scanning confocal microscopy (LSCM, Leica, USA) was used.

### 2.17. *In vitro* BBB model construction and transcytosis assay

Immortalized mouse brain capillary ECs, bEnd.3 cells, were used to generate an *in vitro* BBB model as previously reported.<sup>44</sup> Briefly, bEnd.3 cells were grown on the transwell pre-coated with gelatin (2% w:v) and cultured with DMEM containing 10% FBS as described before. The integrity of the cell monolayer was evaluated by measuring the TEER values using a Millicell-ERS Volt-Ohm Meter (Millipore, USA). When the TEER reached higher than 200 Ω cm<sup>2</sup>, FITC-labeled HF<sub>n</sub>/HF<sub>n</sub>+ (3 μM) in fresh culture medium was added to the apical chamber, and samples from the basal chamber were collected after 2–4 h. The FITC fluorescence intensities (490 nm excitation and 525 nm emission) of each aliquot were measured using a multimodal plate reader (Tecan, Switzerland). The relative transcytosis ratio to HF<sub>n</sub> (%) was defined as the accumulated FITC fluorescence of FITC-HF<sub>n</sub>+ compared with that of FITC-HF<sub>n</sub> when crossing the BBB monolayer.

### 2.18. Native PAGE characterization

The integrity of the FITC-HF<sub>n</sub>+ NPs collected from the basal chamber was also analyzed using native PAGE (PAGE, 5% poly-

acrylamide gels) using freshly prepared FITC-HFn NPs as the control.

### 2.19. Transport across the BBB and knockdown luciferase mRNA of glioma cells

The BBB co-culture model *in vitro* was established to evaluate the penetrating and traversing effects of HFn/HFn+. As before, bEnd.3 cells were seeded on a 24-well cell culture at a density of  $5 \times 10^4$  cells per inserted transwell, and then the TEER was measured until it reached  $200 \Omega \text{ cm}^2$ . Luc-GL261 cells were seeded onto another 24-well plate at a density of  $5 \times 10^4$  cells per well and the bEnd.3 monolayers covered with cell culture were transferred to the plates containing Luc-GL261 cells. After further co-culture for 12 h, siLuc@HFn, siLuc@HFn2, and siLuc@HFn4 ( $3.0 \mu\text{M}$ ) were added on the apical side, and their luciferase knockdown efficiency was measured after 24 h *via* a luciferase assay system protocol as shown before. The knock-out rate relative to HFn (%) was determined after transcytosis.

### 2.20. Statistical analysis

All data from at least three independent experiments were presented as means  $\pm$  standard deviations (SD). The differences between groups were analyzed using Student's test or one-way analysis of variance (ANOVA). In all cases, *p*-values less than 0.05 were considered statistically significance ( $*p < 0.05$ ,  $**p < 0.01$ ,  $***p < 0.001$ ,  $****p < 0.0001$ ).

## 3. Results and discussion

### 3.1. Arginine mutation strategy for HFn+ NPs

A previous study demonstrated that introducing six arginine mutation sites into the inner strands of the O3-33 protein cage could provide a highly positive charge in the lumen.<sup>45</sup> The idea of an attempt to alter inner surface charges of HFn prompted us to select more than six evenly dispersed negatively charged amino acids for the structural mutation to achieve a similar positively charged interior. Rapid advances in computational biology enabled us to readily gain access to the Protein Data Bank (PDB) identification number (ID) of HFn.<sup>46</sup> Using Chimera software, we found all the negatively charged amino acids on the inner surface of the HFn protein structure. Eight residues on the inner surface of the HFn monomer (Asp42, Glu61, Glu64, Glu67, Asp131, Glu134, Asn139, and Asp171) were selectively replaced with arginine

through site-directed mutagenesis to create a class of HFn+ NPs (Table 1), which were expected to have high affinity for anionic siRNAs *via* electrostatic binding. As Chimera showed, a complete 3D morphology of HFn consisted of 24 subunits that can self-assemble into a hollow globular structure with 4-3-2 symmetry (Fig. 1A).<sup>36</sup> The positive and negative charge distributions and the structure of the HFn monomer are illustrated in Fig. 1B and C, respectively. Obviously, all positive charges didn't offset the negative charges and there were more negative charges on the inner surface of subunits.<sup>47</sup> The HFn subunit consists of five helices, a, b, c, d, and e: four long  $\alpha$ -helices (a, b, c, and d) and one tilted short helix (e) connected by a short loop. The 3D model revealed that helices c, d, and e were present at the inner strands of HFn while helices a and b were present at the outer strands. Chimera images presented the subunits of six different types of HFn+, termed HFn1, HFn2, HFn3, HFn4, HFn5, and HFn6 (Fig. 1D). We used a computational protein engineering method to simulate the 3D steric structure model of each HFn+. Simulation results for each protein cage along the fourfold symmetry axis, triple symmetry axis, and superficial three-dimensional structure are shown in Fig. 1E-K. We managed to introduce arginine into the cavity of naive HFn by mutation-induced alteration of the inner surface charge density, which was likely to adjust the binding affinity for siRNA.

In addition, the SIB Bioinformatics Resource Portal tool was used to predict the isoelectric point (pI) of proteins, and the prediction results demonstrated that the theoretical pI values of HFn+ variants (pI = 7.42–8.92) were higher than that of HFn (pI = 5.30). This significant difference facilitated the encapsulation of siRNA as the interior surface of HFn+ remained positively charged during the process of disassembly and reassembly, thus providing an electrostatic force to promote gene encapsulation (Table 1).

### 3.2. Preparation and characterization of HFn+ NPs

Building on the computer structural simulation, we identified eight mutation residues and chose six HFn+ variants with different mutation levels for further study. They were all expressed in *Escherichia coli* (BL21(DE3)) as previously described.<sup>48,49</sup> With slight modification and optimization during plasmid construction, we fused a 6 $\times$  His-tag to the N-terminus of HFn for HisTrap<sup>TM</sup> purification, followed by SEC methods, which ensured the high purity of these HFn+ NPs.

**Table 1** The specific arginine mutation sites on the inner surface of HFn and the prediction of the theoretical pI of HFn+

Identity	Number of mutations	Arginine mutation sites	Theoretical value of pI
HFn1	8	D(Asp42), E(Glu61), E(Glu64), E(Glu67), D(Asp131), E(Glu134), N(Asn139), D(Asp171)	8.92
HFn2	7	D(Asp42), E(Glu61), E(Glu64), E(Glu67), D(Asp131), N(Asn139), D(Asp171)	8.71
HFn3	7	D(Asp42), E(Glu61), E(Glu64), E(Glu67), E(Glu134), N(Asn139), D(Asp171)	8.41
HFn4	6	D(Asp42), E(Glu61), E(Glu64), E(Glu67), N(Asn139), D(Asp171)	7.95
HFn5	6	D(Asp42), E(Glu61), E(Glu64), E(Glu67), E(Glu134), D(Asp171)	7.42
HFn6	6	D(Asp42), E(Glu61), E(Glu64), E(Glu67), D(Asp131), N(Asn139)	7.42

The theoretical pI values of HFn+ proteins were calculated using the SIB Bioinformatics Resource Portal tool (<https://web.expasy.org/protparam/>).

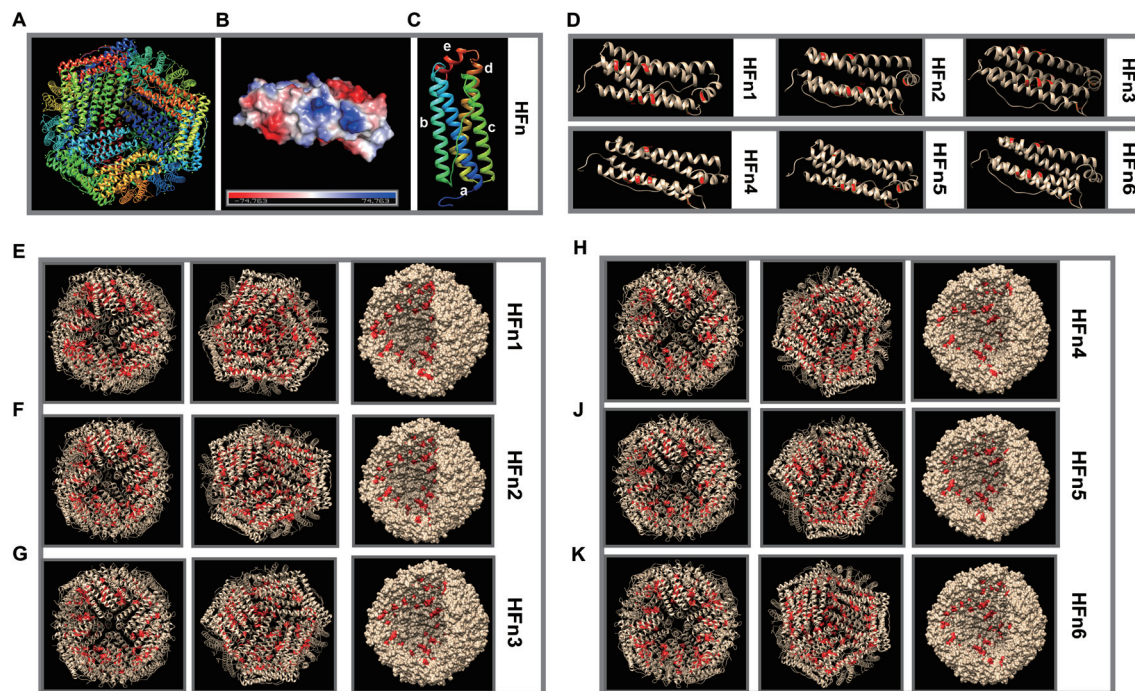


**Fig. 1** Design of the supercharged HFfn NPs. (A) Wild-type HFfn (PDB ID: 3AJ0) with 24 monomers displayed in different colors. (B) The charge distribution of the HFfn subunit and (C) the structure of the HFfn subunit (five helices from the NH<sub>2</sub>- and COOH-termini are labelled a, b, c, d, and e, respectively) were generated using Chimera simulation software. (D) The arginine mutation sites on the inner surface of HFfn subunits (gray) are highlighted in red using Chimera, demonstrating the different types of mutations of the HFfn subunit. (E–K) 3D structural models of HFfn+ protein NPs surrounding a fourfold and threefold axis are shown in columns 1 and 2. The surface crystal structures of HFfn+ NPs are shown in column 3 by computer simulation. Six HFfn+ NPs are displayed in total, including HFfn1, HFfn2, HFfn3, HFfn4, HFfn5, and HFfn6. All of the arginine mutation sites are introduced in red.

Their expression and purity were well verified through WB and SDS–PAGE analysis (Fig. 2A). Herein, with normalization of the total protein amount, the WB results demonstrated that the expression of HFfn1 was almost absent; thus, HFfn1 was excluded from further screening. In contrast, the other five HFfn+ variants were clearly observed to have different levels of expression (Fig. 2B). ImageJ was used to compare the production level of each HFfn+ protein semiquantitatively. It is obvious that HFfn2 and HFfn4 exhibited higher yields among the HFfn+ variants (Fig. 2C). Once we had validated the morphology, encapsulation, and biological activity of HFfn2 and HFfn4, we assessed the remaining three proteins.

A clear single HFfn+ protein subunit band was shown at approximately 21 kDa, which was slightly heavier than the molecular weight of HFfn, indicative of successful purification (Fig. 2D and Fig. S2–S5<sup>†</sup>). Up to 90% purity of HFfn+ was achieved according to the ImageJ analysis. Moreover, the BCA assay results showed that purified HFfn2 and HFfn4 had high yields of approximately 80 mg and 55 mg per litre, respectively. TEM morphology showed the homogenous hollow spherical cage-like structures of purified HFfn+ NPs, suggesting that the mutant proteins retained their unique assembly properties (Fig. 2E and Fig. S6<sup>†</sup>). As evidenced by DLS, HFfn+ NPs exhibited a negligible change in average size after mutation (Fig. 2F and 3A). The particle size distribution of 12–18 nm indicated

that HFfn+ was correctly folded and retained many properties similar to those of HFfn, such as self-assembly, stability, non-toxicity, and transcytosis.

### 3.3. Preparation and characterization of siRNA@HFfn or HFfn+ NPs

In addition to the verified structural integrity and high purity, HFfn+ NPs were required to have enough space and flexibility to encapsulate macromolecular NADs. Zhang *et al.*<sup>40</sup> demonstrated that ferritin is rigid under physiological conditions, but turns into a flexible structure when the pH is adjusted to 2–3. siRNA was predicted to be loaded into the cavity of HFfn+ NPs through a pH-mediated disassembly–reassembly procedure to obtain siRNA@HFfn+ NPs. The zeta potentials of the HFfn, HFfn2, HFfn3, HFfn4, HFfn5, and HFfn6 NPs were measured with almost no difference at physiological pH (–9.15 mV to –10.39 mV). At pH 5, which is similar to the pH of the weakly acidic tumor microenvironment (TME),<sup>50</sup> their zeta potential showed negative charge. This result revealed that HFfn+ NPs retained their intact nanostructures when entering the cytoplasm. After the pH was adjusted to 2, the nanostructure was broken down into discrete subunits and the overall charge was positive (Fig. 3B). Additionally, the zeta potentials of all HFfn+ NPs (15.13–22.17 mV) were significantly higher than that of

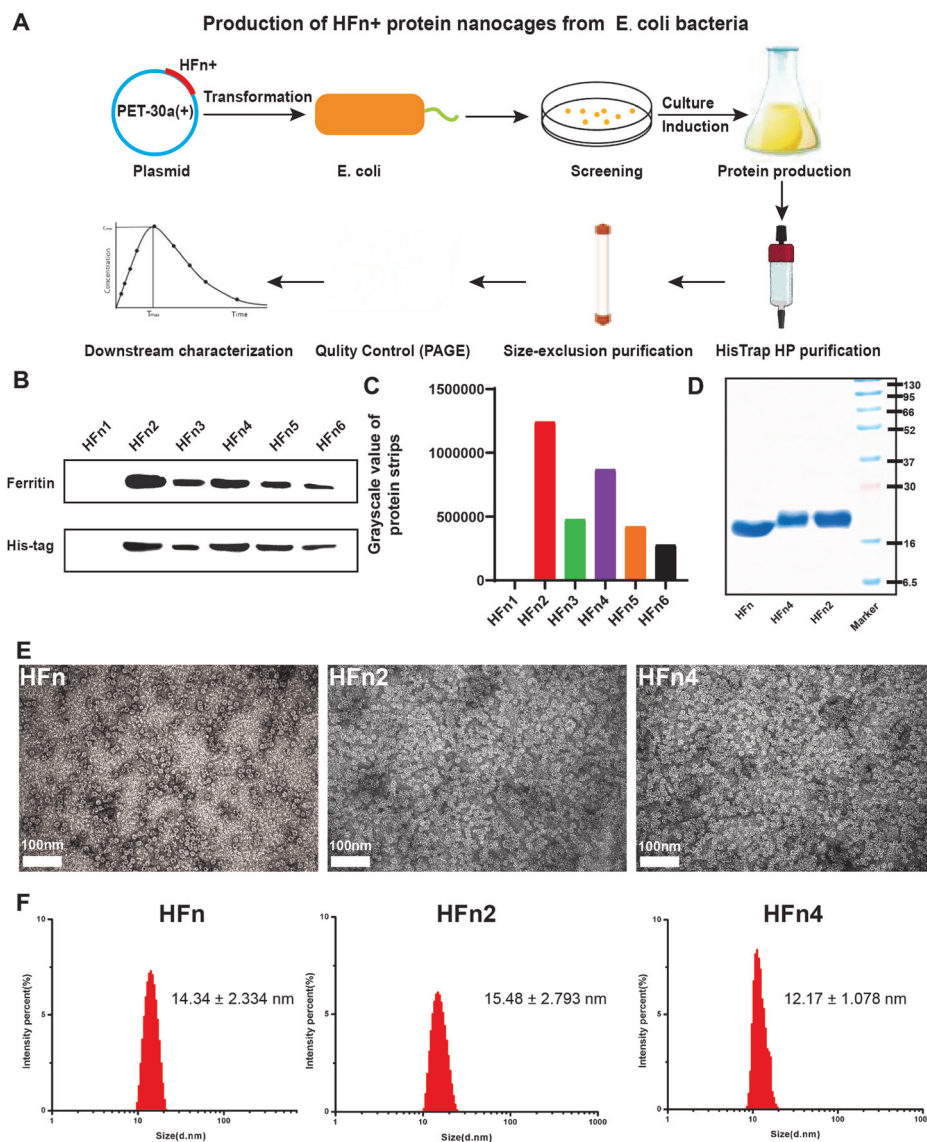


**Fig. 2** Preparation, characterization, and encapsulation verification of HF<sub>n</sub><sup>+</sup> NPs. (A) Scheme for the expression and purification of HF<sub>n</sub><sup>+</sup> in *E. coli*, and subsequent research on HF<sub>n</sub><sup>+</sup>. (B) The expression of HF<sub>n</sub><sup>+</sup> and His-tag from HF<sub>n</sub><sup>+</sup> proteins was evaluated qualitatively by WB detection. (C) Semi-quantitative analysis of the ferritin or His expression levels of HF<sub>n</sub><sup>+</sup> measured using ImageJ. (D) SDS-PAGE for HF<sub>n</sub><sup>+</sup> purity analysis. (E) Representative TEM images of HF<sub>n</sub>, HF<sub>n</sub>2, and HF<sub>n</sub>4 NPs. Scale bars: 100 nm (F) DLS analysis of HF<sub>n</sub>, HF<sub>n</sub>2, and HF<sub>n</sub>4 NPs ( $n = 3$ ).

HF<sub>n</sub> (4.84 mV), probably due to the introduction of positively charged arginine inside the inner surface of HF<sub>n</sub><sup>+</sup> NPs.

To further investigate the formation of their nano-formulations and EE, Cy5-siRNA was chosen as a locator in the process. After removing the unencapsulated RNA using a filter with a molecular cutoff of 100 kDa, we adjusted the pH to 2.0 to disassemble Cy5-siRNA@HF<sub>n</sub> and Cy5-siRNA@HF<sub>n</sub><sup>+</sup> into discrete subunits, and Cy5-siRNA was released from the NPs in the same position as the naked Cy5-siRNA (Fig. 3C). AGE was used to monitor the siRNA of NP-siRNA at a series of siRNA/protein ratios, from 1 : 1 to 1 : 15. The shift of the siRNA location in the gel after being loaded onto NPs showed that maximum encapsulation of siRNAs was achieved when NPs and siRNAs were at the siRNA/protein ratio of 1 : 15. Moreover, the EE (%) of HF<sub>n</sub>

and HF<sub>n</sub><sup>+</sup> NPs loaded with Cy5-siRNA at pH 2 was detected according to the fluorescence intensity of Cy5. Cy5-siRNA@HF<sub>n</sub><sup>+</sup> (10.10–52.83%) possessed a significantly higher EE than HF<sub>n</sub> (6.28–23.96%). A further increase in the siRNA/protein ratio to 1 : 8 enhanced siRNA encapsulation by at least 2.3 times, significantly outperforming naive HF<sub>n</sub> (Table 2). With increasing molar ratios of HF<sub>n</sub>/HF<sub>n</sub><sup>+</sup> to siRNA, EE was observed to increase gradually in a dose-dependent manner. Since no significant EE increase was detected when the siRNA/protein ratio was between 1 : 8 and 1 : 15, the final NP-siRNA was constructed at a siRNA/protein ratio of 1 : 8.

To evaluate the protective effect of HF<sub>n</sub><sup>+</sup> NPs on siRNA, the enzymatic degradation assay of the siRNA@HF<sub>n</sub><sup>+</sup> NPs was conducted at a Cy5-siRNA/protein molar ratio of 1 : 8, and naked



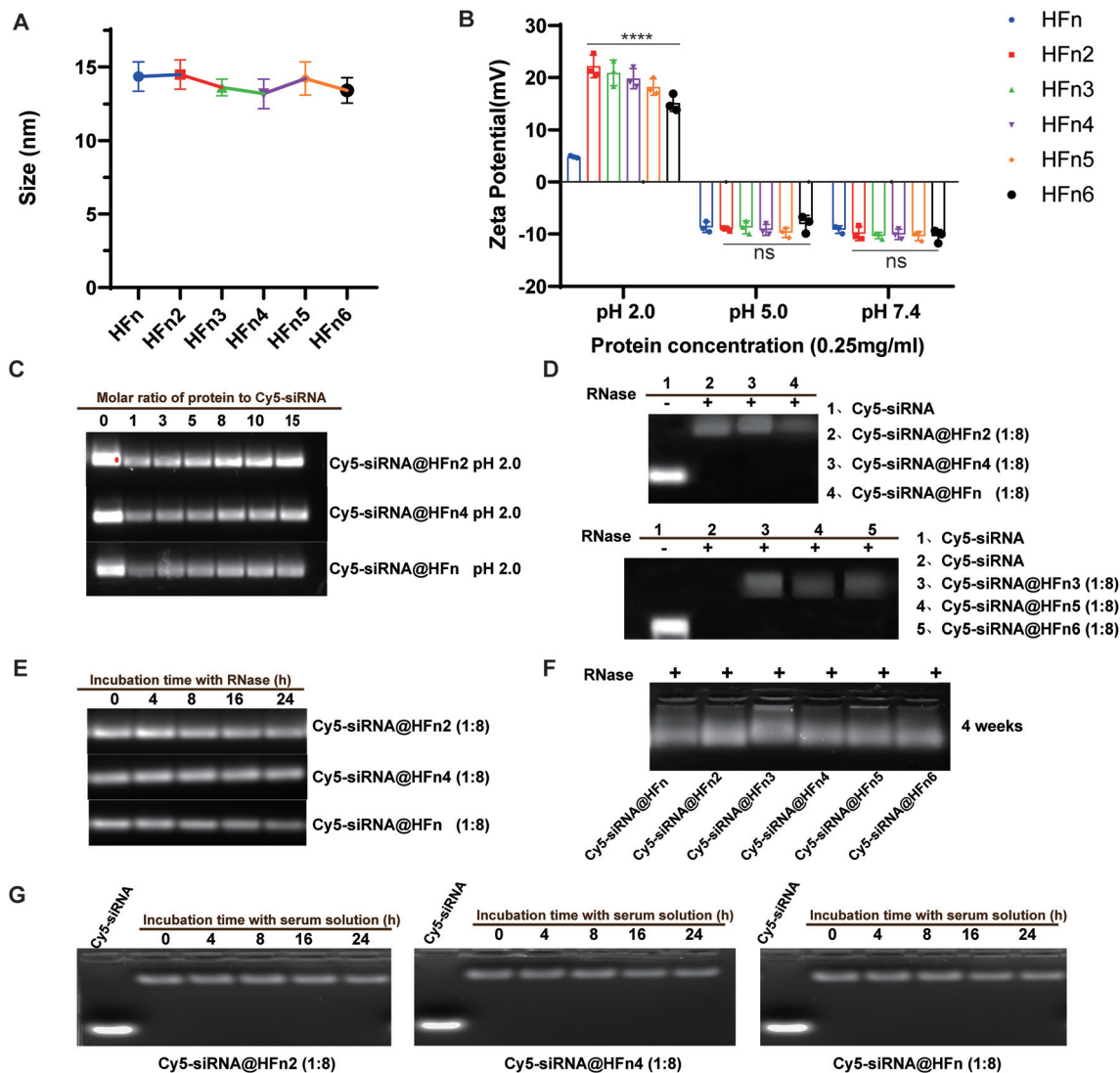


**Fig. 3** (A) DLS diameters of HF n and HF n+ NPs ( $n = 3$ ). (B) Zeta potential of HF n+ NPs in buffers with pH 7.4, 5.0, and 2.0 (PBS, 0.05 M  $\text{PO}_4^{3-}$ , 0.15 M NaCl), respectively ( $n = 3$ ; \*\*\*\* $p < 0.0001$  vs. HF n). (C) The 2% AGE results of Cy5-siRNA@HF n2, Cy5-siRNA@HF n4 and Cy5-siRNA@HF n disassembled in pH 2.0 buffers with encapsulation ratios of 1:1, 1:3, 1:5, 1:8, 1:10, and 1:15, respectively. (D) RNase stability of naked siRNA, Cy5-siRNA@HF n+ and Cy5-siRNA@HF n (1:8) NPs and (E) the co-incubation of HF n2, HF n4 and HF n NPs with RNase A (3 mg  $\text{mL}^{-1}$ ) at 37 °C for 0, 4, 8, 12, 16, and 24 h were detected by AGE. (F) Stability of all Cy5-siRNA@HF n+ and Cy5-siRNA@HF n (1:8) NPs after being stored at 4 °C for four weeks, as detected by AGE. (G) Stability of siRNA@HF n, siRNA@HF n2, and siRNA@HF n4 (1:8) NPs in serum-supplemented medium (10% FBS, pH = 7.4) at 37 °C for 0, 4, 8, 16, and 24 h, as detected by AGE. Significant differences were assessed using a one-way ANOVA with the Tukey test (A and B). Data in (A and B) are presented as means  $\pm$  SD from the second repeat.

siRNA or NP-siRNA was incubated with RNase for different time intervals, followed by 2% AGE. It was confirmed that HF n+ NPs could prevent the enzymatic degradation of nucleic acids and successfully encapsulate siRNA (Fig. 3D). After incubation with RNase A for 0–24 h, the *in vitro* stability of siRNA in the NPs was examined to investigate their resistance to enzymatic degradation. Even after 24 h of incubation with RNase, most siRNAs were still preserved in NP-siRNA as before (Fig. 3E). Then we stored samples in solution at 4 °C for 4 weeks before degrading the RNase with proteinase K. There was no significant decrease in the brightness of the Cy5-siRNA@HF n/HF n+ NP bands after 2% AGE detection (Fig. 3F).

The *in vitro* serum stability of NPs was tested at 37 °C after 24 h of co-incubation. There was no leakage or degradation of siRNA in the NP-siRNA (Fig. 3G). Hence, the siRNA@HF n and siRNA@HF n+ NPs were found to successfully encapsulate siRNA while also protecting it from RNase A degradation.

We monitored the release profiles of Cy5-siRNA from different NPs under acidic and neutral conditions. Over a 92 h period of incubation under physiological conditions (PBS, pH = 7.4), less than 20% Cy5-siRNA was released from HF n, HF n2 or HF n4 NPs, indicating that NPs are sufficiently stable while being transported through the systemic circulation. Under acidic conditions, HF n has been reported to disassemble into

**Table 2** EE (%) evaluation of the Cy5-siRNA@HF<sub>n</sub>+ NPs with different molar ratios of siRNA/protein at 1 : 1, 1 : 3, 1 : 5, 1 : 8, 1 : 10 and 1 : 15

Molar ratio of siRNA to protein	siRNA@HF <sub>n</sub>	siRNA@HF <sub>n</sub> 2	siRNA@HF <sub>n</sub> 3	siRNA@HF <sub>n</sub> 4	siRNA@HF <sub>n</sub> 5	siRNA@HF <sub>n</sub> 6
1 : 1	6.28 ± 0.65	11.10 ± 2.30	12.01 ± 1.05	13.01 ± 0.86	12.05 ± 1.40	10.10 ± 1.06
1 : 3	11.33 ± 0.49*	24.94 ± 4.25*	21.46 ± 3.73**	23.57 ± 2.59**	20.44 ± 2.56*	19.75 ± 2.95*
1 : 5	13.63 ± 1.04*	34.91 ± 2.93***	33.55 ± 1.23**	32.45 ± 0.32***	30.19 ± 1.36**	30.56 ± 0.82**
1 : 8	15.72 ± 0.36**	43.77 ± 4.05***	41.64 ± 3.42***	38.74 ± 2.14***	34.97 ± 3.52***	35.74 ± 2.46***
1 : 10	17.20 ± 1.11**	45.28 ± 2.47***	43.04 ± 2.33****	40.04 ± 2.33****	37.28 ± 2.47***	38.41 ± 1.63***
1 : 15	23.96 ± 2.40**	52.83 ± 4.02***	50.17 ± 3.60****	46.70 ± 3.75****	42.83 ± 3.26***	43.06 ± 3.54****

EE (%) =  $C_i/C_{total} \times 100\%$ , where  $C_i$  is the concentration of the Cy5-siRNA detected by the fluorescence spectrophotometer and  $C_{total}$  represents the concentration of the total added Cy5-siRNA in the NPs. \* $p < 0.05$ , \*\* $p < 0.01$ , \*\*\* $p < 0.001$ , and \*\*\*\* $p < 0.0001$  indicate differences at a molar ratio of 1 : 1 (siRNA : protein). Significant differences were assessed using a one-way ANOVA with Tukey test. Data are presented as means ± SD from the second repeat.

protein subunits and release the encapsulated molecules.<sup>51</sup> As shown in Fig. 4A, the tested NPs showed an initial rapid release of Cy5-siRNA and reached a maximum release of  $86 \pm 3\%$  Cy5-siRNA at 92 h. Compared with HF<sub>n</sub> NPs, HF<sub>n</sub>2 and HF<sub>n</sub>4 NPs showed a slightly slower release at early time points, which is probably due to the internal positive charges in the engineered HF<sub>n</sub>+ NPs. All NPs reached a plateau and presented a similar release profile after 20 h of incubation. Overall, these findings confirmed the pH-dependent kinetics of siRNA release of the developed HF<sub>n</sub>+ NPs.

### 3.4. *In vitro* cytotoxicity evaluation

The safety of delivery systems is of paramount importance to minimize dose-limiting toxicity before clinical studies.<sup>37</sup> We performed safety tests of HF<sub>n</sub>+ on HeLa, GL261 cell lines and primary microglial cells. To determine the safe dose range of HF<sub>n</sub>+ NPs for the following transfection assays, HeLa and GL261 cancer cells were treated with HF<sub>n</sub>2 and HF<sub>n</sub>4 NPs under different concentrations, and the cell survival rate was analyzed using the CCK-8 assay. The cytotoxicity of HF<sub>n</sub>2 and HF<sub>n</sub>4 at concentrations ranging from 0.015 μM to 6.6 μM was detected after co-incubation with the HeLa cells for 6 h, 12 h, and 24 h (Fig. S7A, S7B and S8†). The 3.0 μM cage showed no significant toxicity after 12 h of incubation. However, given that it showed toxicity to HeLa cells under certain conditions (3.0 μM or 6.6 μM, 24 h), we preliminarily identified 3.0 μM as the tolerance dose when co-incubated with HeLa or GL261 cells for 12 h, which can cause minimal toxicity without compromising the transfection efficiency. The cytotoxicity assay results for HF<sub>n</sub>2 and HF<sub>n</sub>4 in GL261 cells after 12 h in the same concentration range (0.015–3.0 μM) confirmed our hypothesis, revealing that this transfection condition (3.0 μM, 12 h) was suitable for GL261 cells (Fig. S7C†). After 12 h of co-incubation, the cytotoxicity of the other three HF<sub>n</sub>+ NPs (HF<sub>n</sub>3, HF<sub>n</sub>5, HF<sub>n</sub>6) in both HeLa and GL261 cells was measured at a concentration of 3.0 μM, confirming that the functionalization of arginine in the interior cavity of HF<sub>n</sub> had no significant toxicity up to 3.0 μM cage in either cell (Fig. S7D†). To further conclusively demonstrate the toxicity, we also tested the toxicity of NPs using primary microglial cells in the concentration range 0–4 μM, NPs didn't show sig-

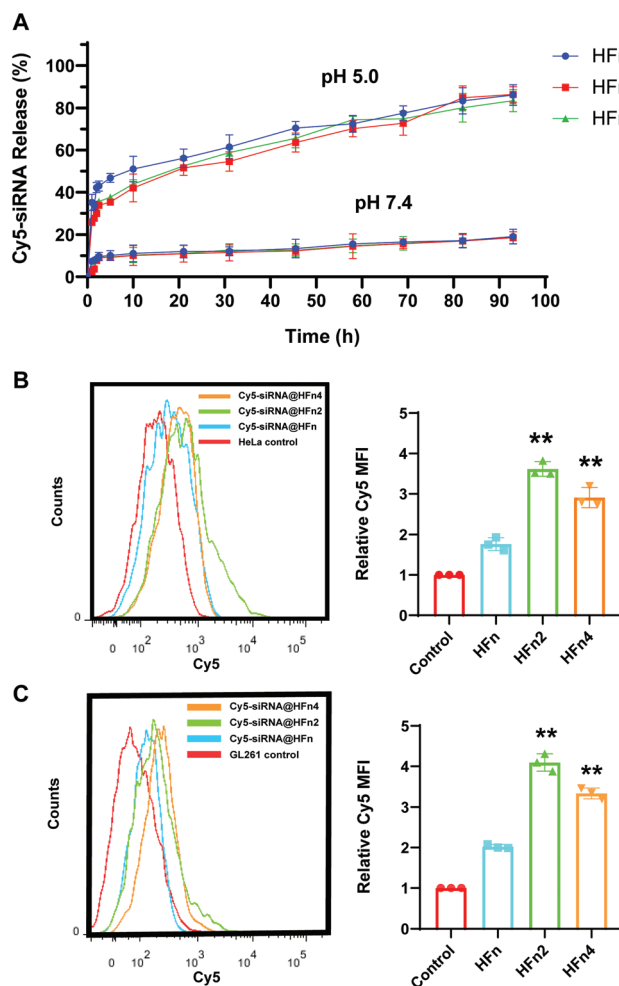


**Fig. 4** Cy5-siRNA release kinetics and cellular uptake of Cy5-siRNA@HF<sub>n</sub>+ NPs in Dual-Luc-HeLa cells and Luc-GL261 cells. (A) *In vitro* release profile of the Cy5-siRNA from HF<sub>n</sub>, HF<sub>n</sub>2, and HF<sub>n</sub>4 NPs at pH 5.0 and pH 7.4 at 37 °C ( $n = 3$ , bars represent means ± SD). Flow cytometry analysis of the uptake of Cy5-siRNA@HF<sub>n</sub> and Cy5-siRNA@HF<sub>n</sub>+ (Cy5-siRNA@HF<sub>n</sub>2, Cy5-siRNA@HF<sub>n</sub>4) in (B) HeLa cells and (C) GL261 cells ( $n = 3$ ; \*\* $p < 0.01$  vs. Cy5-siRNA@HF<sub>n</sub>). Significant differences were assessed using a one-way ANOVA with the Tukey test (B and C). Data in (B and C) are presented as means ± SD from the second repeat.

nificant toxicity below 3.0  $\mu\text{M}$  after co-incubation for 12 h (Fig. S9†).

### 3.5. Quantitative cellular uptake of siRNA@HF<sub>n</sub>+ NPs

We next examined whether arginine mutation could contribute to more efficient cellular uptake of HF<sub>n</sub> NPs. Flow cytometry

was used to evaluate the cellular internalization of Cy5-siRNA@HF<sub>n</sub>+ NPs in HeLa and GL261 cells. Herein, the cellular uptake of Cy5-siRNA@HF<sub>n</sub>+ in either cell at a concentration of 1.5  $\mu\text{M}$  was detected in the first round of screening (Fig. S10†). Flow cytometry analysis revealed that the cellular mean fluorescence intensity (MFI) of Cy5-siRNA@HF<sub>n</sub>+ was

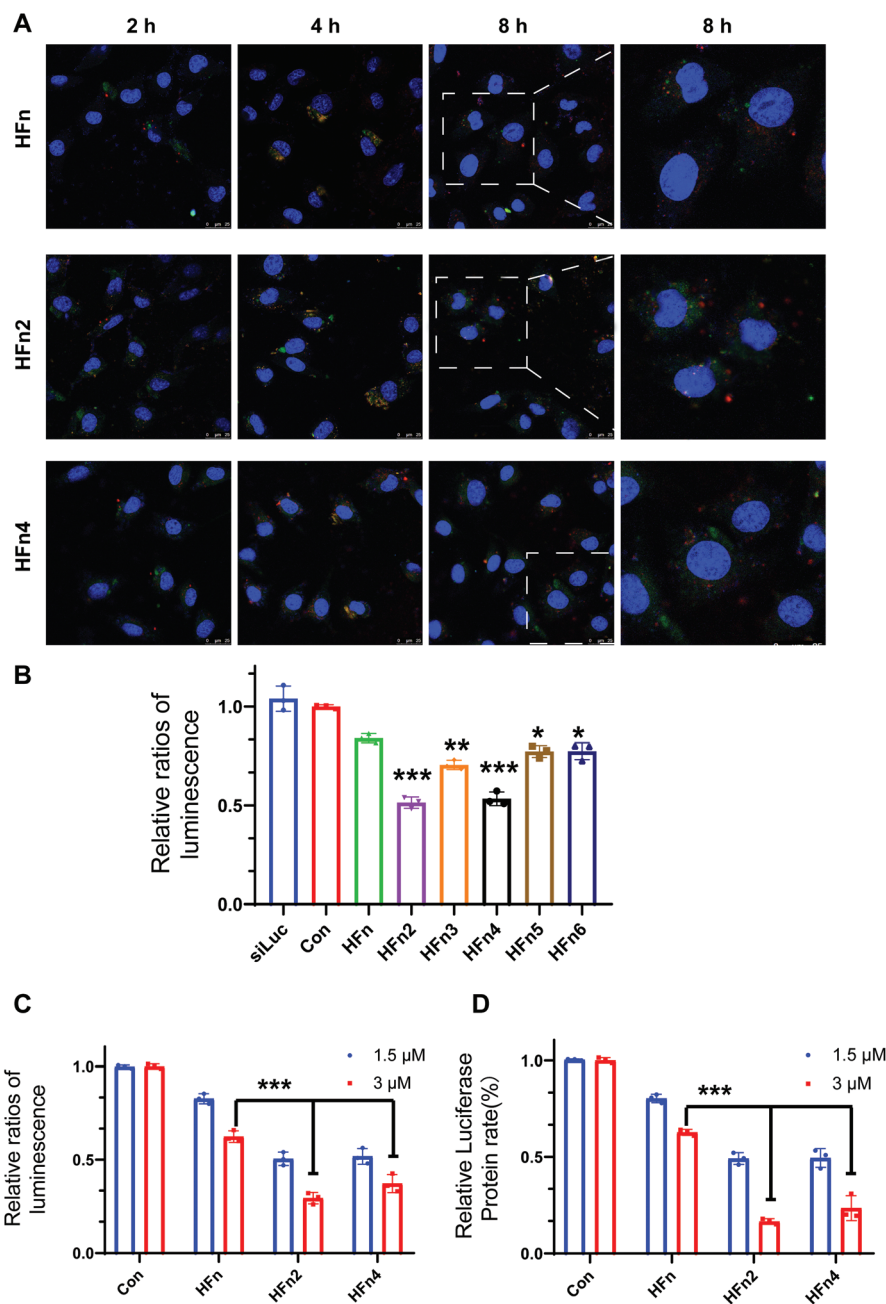


**Fig. 5** Endosomal escape capacity of NPs in GL261 cells and gene silencing efficiency in Dual-Luc-HeLa cells and Luc-GL261 cells. (A) Endosome escape of Cy5-siRNA (red)-loaded HF<sub>n</sub>, HF<sub>n</sub>2, and HF<sub>n</sub>4 NPs after incubation with GL261 cells for 2, 4, and 8 h. Nuclei were stained with DAPI (blue), and late endosomes were stained with Lyso-Tracker Green (green). Scale bars: 25  $\mu\text{m}$ . (B) Firefly luminescence ratio in Dual-Luc HeLa cells after transfection with 1.5  $\mu\text{M}$  siLuc@HF<sub>n</sub>+ NPs at a 1 : 8 ratio ( $n = 3$ ;  $**p < 0.01$  vs. Cy5-siRNA@HF<sub>n</sub>). (C) Relative firefly luciferase expression in Dual-Luc HeLa cells transfected with siLuc@HF<sub>n</sub>/HF<sub>n</sub>2/HF<sub>n</sub>4 NPs at an elevated dose of NPs (3.0  $\mu\text{M}$ ) at a 1 : 8 ratio ( $n = 3$ ). (D) The same dose was used in Luc-GL261 cells ( $n = 3$ ;  $*p < 0.05$ ,  $**p < 0.01$ ,  $***p < 0.001$  vs. siLuc@HF<sub>n</sub>). Significant differences were assessed using a one-way ANOVA with the Tukey test (B–D). Data in (B–D) are presented as means  $\pm$  SD from the second repeat.

significantly stronger than the MFI of the control, indicating that more HF<sub>n</sub>+ NPs were internalized. In addition, we found that GL261 cells took up more Cy5-siRNA@HF<sub>n</sub>+ than HeLa cells, presumably due to the differences in the expression of TfR1 on these two cells. The cellular internalization of all five HF<sub>n</sub>+ NPs significantly exceeded that of HF<sub>n</sub>. Among NPs, HF<sub>n</sub>2, HF<sub>n</sub>4, and HF<sub>n</sub>3 were clearly superior to the other variants. Due to the low productivity of HF<sub>n</sub>3 and its unremarkable cell binding ability, we further investigated the cellular uptake of HF<sub>n</sub>2 and HF<sub>n</sub>4 instead of HF<sub>n</sub>3 in both HeLa and GL261 cells at a higher concentration of 3.0 μM (Fig. 4B and C). There were significant fluorescence signal differences in the MFI between HF<sub>n</sub>+ (HF<sub>n</sub>2, HF<sub>n</sub>4) and HF<sub>n</sub> treated groups while there was no statistical difference between HF<sub>n</sub>2 and HF<sub>n</sub>4. Together, these internalization results demonstrated that the different positions of HF<sub>n</sub> where arginine residue mutations occurred may affect the binding affinity to different epitopes on TfR1.<sup>52</sup> HF<sub>n</sub>2, HF<sub>n</sub>3, and HF<sub>n</sub>4 possessed the preferred encapsulation capability and enhanced cellular uptake, and are promising for development to facilitate siRNA delivery in the brain. However, considering the drawbacks of HF<sub>n</sub>3, we excluded it from the following assays.

### 3.6. Endosomal escape property

To enable siRNA-mediated gene silencing, NPs need to facilitate siRNA escape from endosomes followed by release into

the cytoplasm.<sup>10</sup> As shown in Fig. 5A, we observed that Cy5-siRNA@NPs entered GL261 cells rapidly and were partially located in endosomes after 2 h of incubation. The internalized Cy5-siRNA NPs (red) were mainly colocalized with late endosomes (green) at 4 h of incubation, and most of the NPs were located outside of the endosomes after another 4 h of incubation, indicating the release of the siRNA into the cytoplasm (Fig. 5A). The confocal images demonstrated that HF<sub>n</sub>2 and HF<sub>n</sub>4 NPs were able to escape from endosomes after 8 h of incubation with GL261 cells.

### 3.7. *In vitro* gene silencing efficacy of siRNA@HF<sub>n</sub>+ NPs

It is worthwhile to further investigate the gene silencing efficacy of siRNA@HF<sub>n</sub>+ NPs at the cellular level due to their outstanding EE and binding affinity. We evaluated the *in vitro* gene silencing efficacy of siLuc@HF<sub>n</sub>+ NPs in Dual-Luc HeLa cells and Luc-GL261 cells. Dual-Luc HeLa cells were genetically engineered to stably express both firefly and *Renilla* luciferase, whereas Luc-GL261 cells expressed only firefly luciferase. At the initial screening, 1.5 μM siLuc@HF<sub>n</sub>+ NPs were incubated with Dual-Luc HeLa cells, and the expression of both reporter proteins was measured after 24 h post-transfection. Significant luciferase knockdown of approximately 50% and 45% was achieved after treatment with siLuc@HF<sub>n</sub>2 and siLuc@HF<sub>n</sub>4 NPs, respectively. In contrast, the siLuc@HF<sub>n</sub> NPs (~20%) exhibited a significant decrease in the luciferase knockdown

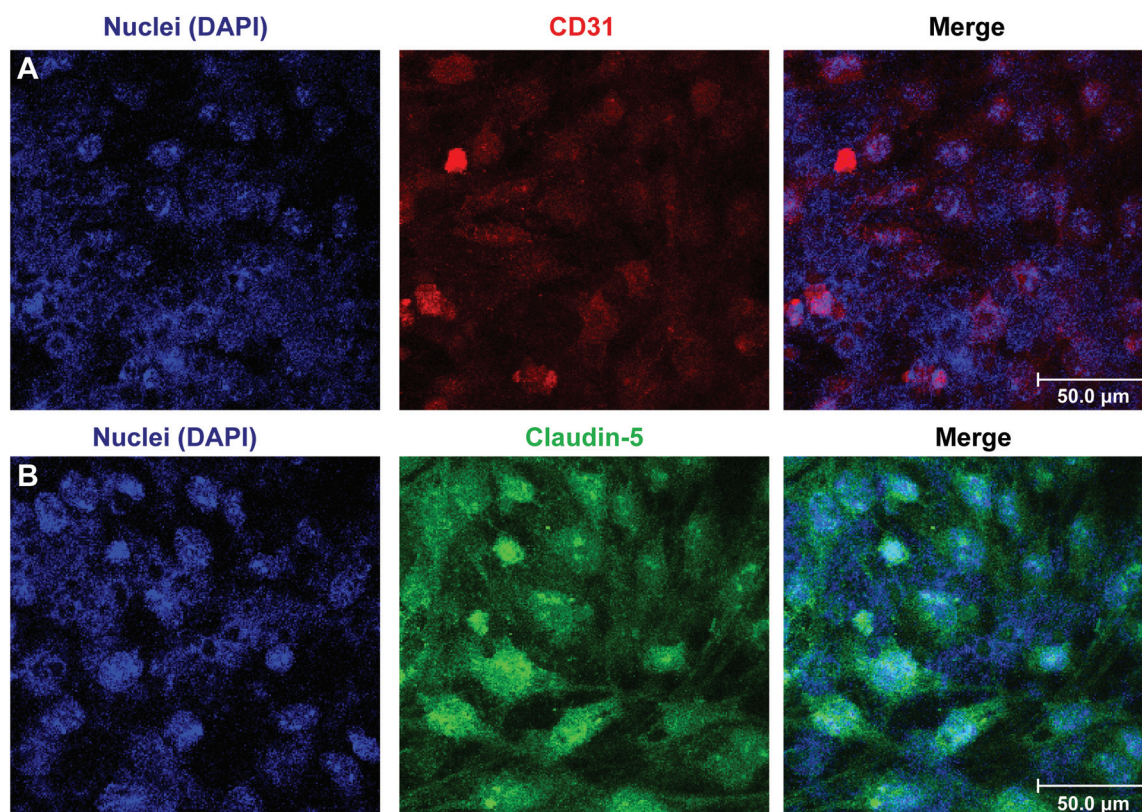


Fig. 6 (A) Immunostaining of a bEnd.3 monolayer for endothelial cell marker CD31 (red). (B) Immunostaining of a bEnd.3 monolayer for tight junction marker claudin-5 (green). Cells were counterstained with cell nucleus dye DAPI (blue). Scale bars: 50 μm.

efficacy (Fig. 5B). The NP-mediated luciferase knockdown was dose-dependent when the loading concentration of luciferase siRNA increased to 3  $\mu\text{M}$ , especially for siLuc@HF<sub>n</sub>2 and siLuc@HF<sub>n</sub>4 NPs (Fig. 5C and D). No significant fluctuation of *Renilla* luciferase intensity (internal control) was observed during the down-regulation of luciferase, indicating that HF<sub>n</sub>2 and HF<sub>n</sub>4 NPs were not cytotoxic. The difference in the gene silencing efficiencies of HF<sub>n</sub> and HF<sub>n</sub>2 or HF<sub>n</sub>4 NPs may be partly attributed to the cellular uptake efficiency. These results demonstrate that siRNA@HF<sub>n</sub>+ NPs have the potential to silence target genes with high efficiency.

### 3.8. Integrity of *in vitro* BBB model

The *in vitro* BBB model recapitulates a number of characteristics, including the expression of specific endothelial markers and BBB transporter proteins, and the formation of monolayers with high TEER, indicating the presence of tight junctions.<sup>53</sup> The *in vitro* models derived from primary cerebral microvessels from various species carried an inherent problem of contamination, slow growth, and de-differentiation. Immortalized mouse brain microvessel endothelial cell lines,

bEnd.3 cells, were used to establish an *in vitro* BBB monoculture model since they can express several proteins responsible for the BBB penetration of xenobiotics.<sup>54</sup> In fact, bEnd.3 monocultures have been extensively used to construct *in vitro* BBB models in many published journals.<sup>1,54–58</sup> Astrocytes and pericytes only provide ~20% of the resistance to various-sized solutes while the endothelium provides ~75–80% of the *in vitro* BBB resistance.<sup>58</sup> Additionally, there is no significant difference between bEnd.3 monoculture model and cocultures comprising mouse brain endothelial cells and astrocytes in terms of many barrier properties (hydraulic conductivity, diffusive solute permeability, *etc.*). On day 4, when the TEER reached 200  $\Omega\text{ cm}^2$ , we examined the expression of endothelial cell markers and tight junction proteins in the endothelial monolayer. As shown in Fig. 6A, immunostaining of bEnd.3 monolayer showed expression of endothelial cell marker CD31 and provided evidence of cell adhesion, which is consistent with previous reports.<sup>59,60</sup> Tight junction transmembrane protein claudin-5 expressed on bEnd.3 monolayer indicated the well-formed confluent monolayer on the luminal side of the transwell (Fig. 6B).<sup>61</sup> The immunofluorescence

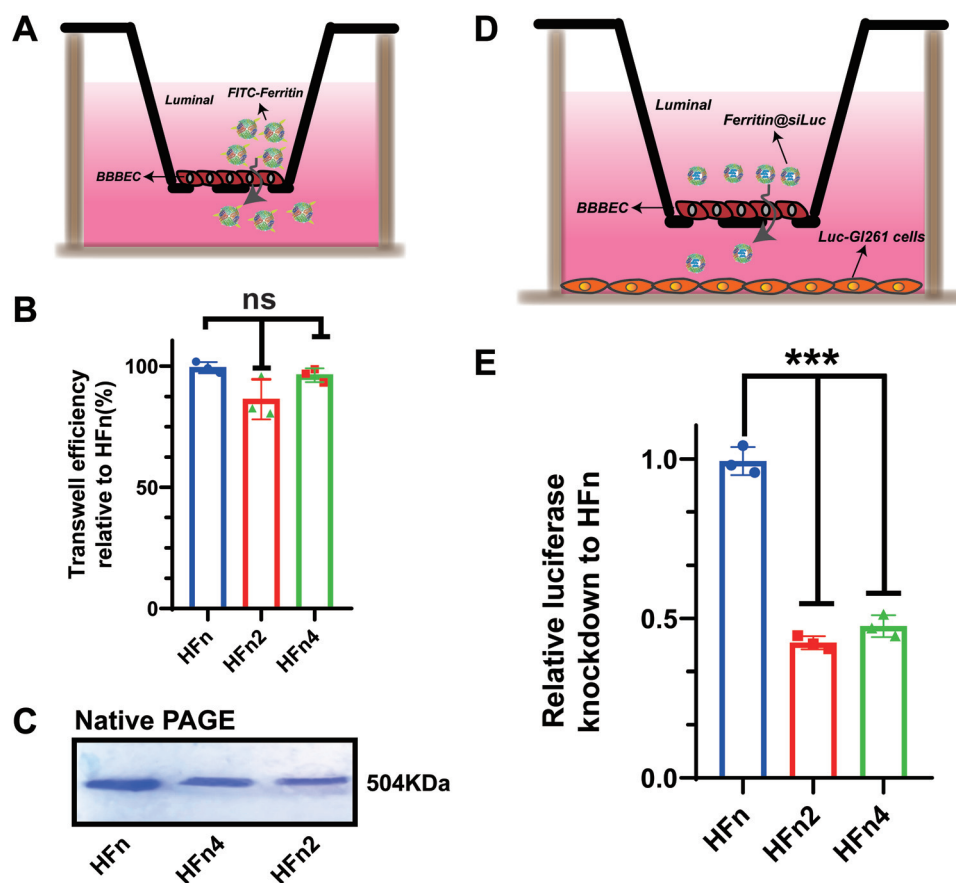


**Fig. 7** siLuc@HF<sub>n</sub>+ NPs successfully traversed the BBB and knocked down luciferase expression while maintaining their structure intact after passing through BBB ECs. (A) Schematic illustration of the *in vitro* BBB model. (B) Transcytosis efficiency of HF<sub>n</sub>, HF<sub>n</sub>2, and HF<sub>n</sub>4 in an *in vitro* BBB model ( $n = 3$ ). (C) Native PAGE analysis of the traversed HF<sub>n</sub>, HF<sub>n</sub>2, and HF<sub>n</sub>4 samples from the basal chamber. (D) Schematic illustration of a co-culture model involving bEnd.3 and Luc-GL261 cells to mimic the BBB and TME. (E) The relative luciferase knockdown efficiency of HF<sub>n</sub>2 and HF<sub>n</sub>4 to HF<sub>n</sub> in cancer cells after traversing the BBB ( $n = 3$ ;  $p > 0.05$  (ns),  $***p < 0.001$  vs. siLuc@HF<sub>n</sub>). Significant differences were assessed using a one-way ANOVA with the Tukey test (B and E). Data in (B and E) are presented as means  $\pm$  SD from the second repeat.

images suggested successful construction of the *in vitro* BBB model that will be used in the following experiments.

### 3.9. *In vitro* gene silencing effects of HF<sub>n</sub>+ NPs after traversing the BBB

Due to their higher knockdown efficiency in Luc-GL261 cells, HF<sub>n</sub>2 and HF<sub>n</sub>4 emerged as promising vectors for gene delivery to the brain and merited further investigation of their transcytosis ability. We constructed an *in vitro* BBB model using bEnd.3 cells as previously described (Fig. 7A). It was observed that the transcytosis efficiency of HF<sub>n</sub>2 and HF<sub>n</sub>4 NPs slightly decreased compared with naive HF<sub>n</sub> NPs, but they showed no statistical difference (Fig. 7B). Aliquots from the basolateral side of the inserts were collected and tested using native PAGE. The bands with a theoretical molecular weight of 504 kDa confirmed that the NPs retained their structural integrity after crossing the BBB monolayer, which is essential to avoid the undesirable leakage of siRNA that may occur when crossing the BBB (Fig. 7C).

To further study the luciferase knockdown efficiency of HF<sub>n</sub>2 and HF<sub>n</sub>4 in Luc-GL261 cells after traversing the BBB, we designed a co-culture model consisting of bEnd.3 and Luc-GL261 cells to mimic the TME and BBB (Fig. 7D). As shown in Fig. 7E, despite the lower transcytosis efficiency of HF<sub>n</sub>2 in comparison with HF<sub>n</sub>4, its knockdown efficiency increased by 57% compared with HF<sub>n</sub> and slightly outperformed HF<sub>n</sub>4. Overall, HF<sub>n</sub>2 was identified as a promising nanocarrier candidate for siRNA delivery into the brain.

## 4. Conclusion

In summary, a simple yet elegant electrostatic encapsulation strategy based on an arginine mutation on the inner surface of HF<sub>n</sub> was adopted which provided a solution to the issue of low siRNA encapsulation and a new modality in which to modify protein cages for therapeutic cargo delivery. HF<sub>n</sub>2, the optimal HF<sub>n</sub>+ variant screened among HF<sub>n</sub>+ NPs, increased luciferase knockdown efficiency compared with naive HF<sub>n</sub> after traversing the BBB. Moreover, compared with other HF<sub>n</sub>+ NPs, HF<sub>n</sub>2 was readily produced in *E. coli* at a high yield (approximately 80 mg L<sup>-1</sup> with purity up to 90% in this work) and exhibited almost no toxicity. While this nanocarrier still needs to be further explored, optimized, and engineered, our findings reveal that the genetic manipulation of HF<sub>n</sub> can effectively improve the EE of siRNA, promoting the development of functionalized protein NPs toward BBB-traversing gene delivery.

## Author contributions

Xue-Qing Zhang, Xiaoyang Xu and Ziwei Yuan conceived the study and designed experiments. Xue-Qing Zhang supervised the research throughout. Ziwei Yuan and Bin Wang carried out the experiments and analyzed the data. Ziwei Yuan and Bin

Wang wrote the manuscript. Ziwei Yuan performed all the statistical analysis. Yilong Teng, William Ho, Bin Hu and Kofi Oti Boakye-Yiadom reviewed the manuscript. Xiaoyang Xu and Ziwei Yuan edited and revised the manuscript.

## Conflicts of interest

There are no conflicts to declare.

## Acknowledgements

The work was funded by the Interdisciplinary Program of Shanghai Jiao Tong University (project number ZH2018ZDA36 (19X190020006)), Shanghai Jiao Tong University Scientific and Technological Innovation Funds (2019TPA10), and the Foundation of National Facility for Translational Medicine (Shanghai) (TMSK-2020-008). Xiaoyang Xu acknowledges support from the American Heart Association (19AIREA34380849), the National Science Foundation (2001606) and the Gustavus and Louise Pfeiffer Research Foundation Award. We thank Xiyun Yan (Institute of Biophysics, CAS) for her generous gift of pET-HF<sub>n</sub> plasmid and are grateful to Kelong Fan (Institute of Biophysics, CAS) for his professional suggestions on protein purification.

## References

- 1 K. Fan, X. Jia, M. Zhou, K. Wang, J. Conde, J. He, J. Tian and X. Yan, *ACS Nano*, 2018, **12**, 4105–4115.
- 2 Y. J. Zuchero, X. Chen, N. Bien-Ly, D. Bumbaca, R. K. Tong, X. Gao, S. Zhang, K. Hoyte, W. Luk, M. A. Huntley, L. Phu, C. Tan, D. Kallop, R. M. Weimer, Y. Lu, D. S. Kirkpatrick, J. A. Ernst, B. Chih, M. S. Dennis and R. J. Watts, *Neuron*, 2016, **89**, 70–82.
- 3 Y. Jiang, J. Zhang, F. Meng and Z. Zhong, *ACS Nano*, 2018, **12**, 11070–11079.
- 4 N. Weiss, F. Miller, S. Cazaubon and P. O. Couraud, *Biochim. Biophys. Acta*, 2009, **1788**, 842–857.
- 5 C. Saraiva, C. Praca, R. Ferreira, T. Santos, L. Ferreira and L. Bernardino, *J. Controlled Release*, 2016, **235**, 34–47.
- 6 L. Naldini, *Nature*, 2015, **526**, 351–360.
- 7 D. Kwon, *Nature*, 2021, **592**, 180–183.
- 8 L. Alvarez-Erviti, Y. Seow, H. Yin, C. Betts, S. Lakhali and M. J. Wood, *Nat. Biotechnol.*, 2011, **29**, 341–345.
- 9 S. F. Dowdy, *Nat. Biotechnol.*, 2017, **35**, 222–229.
- 10 G. Sahay, W. Querbes, C. Alabi, A. Eltoukhy, S. Sarkar, C. Zurenko, E. Karagiannis, K. Love, D. Chen, R. Zoncu, Y. Buganim, A. Schroeder, R. Langer and D. G. Anderson, *Nat. Biotechnol.*, 2013, **31**, 653–658.
- 11 Q. Huang, K. Y. Chan, I. G. Tobey, Y. A. Chan, T. Poterba, C. L. Boutros, A. B. Balazs, R. Daneman, J. M. Bloom, C. Seed and B. E. Deverman, *PLoS One*, 2019, **14**, e0225206.
- 12 B. E. Deverman, P. L. Pravdo, B. P. Simpson, S. R. Kumar, K. Y. Chan, A. Banerjee, W. L. Wu, B. Yang, N. Huber,

- S. P. Pasca and V. Gradinaru, *Nat. Biotechnol.*, 2016, **34**, 204–209.
- 13 E. J. Lee, N. K. Lee and I. S. Kim, *Adv. Drug Delivery Rev.*, 2016, **106**, 157–171.
- 14 M. Uchida, M. T. Klem, M. Allen, P. Suci, M. Flenniken, E. Gillitzer, Z. Varpness, L. O. Liepold, M. Young and T. Douglas, *Adv. Mater.*, 2007, **19**, 1025–1042.
- 15 S. Bhaskar and S. Lim, *NPG Asia Mater.*, 2017, **9**, e371.
- 16 K. Fan, C. Cao, Y. Pan, D. Lu, D. Yang, J. Feng, L. Song, M. Liang and X. Yan, *Nat. Nanotechnol.*, 2012, **7**, 459–464.
- 17 L. Li, M. Munoz-Culla, U. Carmona, M. P. Lopez, F. Yang, C. Trigueros, D. Otaegui, L. Zhang and M. Knez, *Biomaterials*, 2016, **98**, 143–151.
- 18 M. Truffi, L. Fiandra, L. Sorrentino, M. Monieri, F. Corsi and S. Mazzucchelli, *Pharmacol. Res.*, 2016, **107**, 57–65.
- 19 J. He, K. Fan and X. Yan, *J. Controlled Release*, 2019, **311–312**, 288–300.
- 20 M. Bellini, S. Mazzucchelli, E. Galbiati, S. Sommaruga, L. Fiandra, M. Truffi, M. A. Rizzuto, M. Colombo, P. Tortora, F. Corsi and D. Prosperi, *J. Controlled Release*, 2014, **196**, 184–196.
- 21 B. Jiang, X. Chen, G. Sun, X. Chen and K. Fan, *Nano Today*, 2020, **35**, 100948.
- 22 B. R. Lee, H. K. Ko, J. H. Ryu, K. Y. Ahn, Y. H. Lee, S. J. Oh, J. H. Na, T. W. Kim, Y. Byun, I. C. Kwon, K. Kim and J. Lee, *Sci. Rep.*, 2016, **6**, 35182.
- 23 P. Santambrogio, A. Cozzi, S. Levi, E. Rovida, F. Magni, A. Albertini and P. Arosio, *Protein Expression Purif.*, 2000, **19**, 212–218.
- 24 M. D. Lawson and J. P. Artymiuk, *Nature*, 1991, **349**, 541–541.
- 25 K. Iwahori, K. Yoshizawa, M. Muraoka and I. Yamashita, *Inorg. Chem.*, 2005, **44**, 6393–6400.
- 26 T. Beck, S. Tetter, M. Kunzle and D. Hilvert, *Angew. Chem., Int. Ed.*, 2015, **54**, 937–940.
- 27 P. M. Harrison and P. Arosio, *Biochim. Biophys. Acta*, 1996, **1275**, 161–203.
- 28 H. Huang, S. Yuan, Z. Ma, P. Ji, X. Ma, Z. Wu and X. Qi, *Biomater. Sci.*, 2020, **8**, 1759–1770.
- 29 I. Inoue, M. Chiba, K. Ito, Y. Okamatsu, Y. Suga, Y. Kitahara, Y. Nakahara, Y. Endo, K. Takahashi, U. Tagami and N. Okamoto, *Nanoscale*, 2021, **13**, 1875–1883.
- 30 Z. Yang, X. Wang, H. Diao, J. Zhang, H. Li, H. Sun and Z. Guo, *Chem. Commun.*, 2007, **33**, 3453.
- 31 M. Liang, K. Fan, M. Zhou, D. Duan, J. Zheng, D. Yang, J. Feng and X. Yan, *Proc. Natl. Acad. Sci. U. S. A.*, 2014, **111**, 14900–14905.
- 32 H. Huang, K. Sha, H. Veroniaina, Z. Wu, Z. Wu and X. Qi, *Nanoscale*, 2020, **12**, 7347–7357.
- 33 A. E. Powell, K. Zhang, M. Sanyal, S. Tang, P. A. Weidenbacher, S. Li, T. D. Pham, J. E. Pak, W. Chiu and P. S. Kim, *ACS Cent. Sci.*, 2021, **7**, 183–199.
- 34 S. Tetter and D. Hilvert, *Angew. Chem., Int. Ed.*, 2017, **56**, 14933–14936.
- 35 R. Zschoche and D. Hilvert, *J. Am. Chem. Soc.*, 2015, **137**, 16121–16132.
- 36 Y. Jin, J. He, K. Fan and X. Yan, *Nanoscale*, 2019, **11**, 12449–12459.
- 37 M. Kih, E. J. Lee, N. K. Lee, Y. K. Kim, K. E. Lee, C. Jeong, Y. Yang, D. H. Kim and I. S. Kim, *Biomaterials*, 2018, **180**, 67–77.
- 38 E. J. Lee, G. H. Nam, N. K. Lee, M. Kih, E. Koh, Y. K. Kim, Y. Hong, S. Kim, S. Y. Park, C. Jeong, Y. Yang and I. S. Kim, *Adv. Mater.*, 2018, **30**, 1705581.
- 39 K. T. Love, K. P. Mahon, C. G. Levins, K. A. Whitehead, W. Querbes, J. R. Dorkin, J. Qin, W. Cantley, L. L. Qin, T. Racie, M. Frank-Kamenetsky, K. N. Yip, R. Alvarez, D. W. Sah, A. de Fougères, K. Fitzgerald, V. Koteliansky, A. Akinc, R. Langer and D. G. Anderson, *Proc Natl Acad Sci USA*, 2010, **107**, 1864–1869.
- 40 S. Zhang, J. Zang, H. Chen, M. Li, C. Xu and G. Zhao, *Small*, 2017, **13**, 1701045.
- 41 M. Kim, Y. Rho, K. S. Jin, B. Ahn, S. Jung, H. Kim and M. Ree, *Biomacromolecules*, 2011, **12**, 1629–1640.
- 42 X. T. Ji, H. Lin and H. Q. Huang, *J. Proteomics*, 2012, **75**, 3145–3157.
- 43 S. W. Young, M. Stenzel and J. L. Yang, *Crit. Rev. Oncol. Hematol.*, 2016, **98**, 159–169.
- 44 M. Zhai, Y. Wang, L. Zhang, M. Liang, S. Fu, L. Cui, M. Yang, W. Gong, Z. Li, L. Yu, X. Xie, C. Yang, Y. Yang and C. Gao, *Drug Delivery*, 2018, **25**, 1013–1024.
- 45 T. G. W. Edwardson, T. Mori and D. Hilvert, *J. Am. Chem. Soc.*, 2018, **140**, 10439–10442.
- 46 W. L. Hsu, C. J. Oldfield, B. Xue, J. Meng, F. Huang, P. Romero, V. N. Uversky and A. K. Dunker, *Protein Sci.*, 2013, **22**, 258–273.
- 47 S. Yin, B. Zhang, J. Lin, Y. Liu, Z. Su and J. Bi, *Eng. Life Sci.*, 2021, **21**, 630–642.
- 48 M. Liang, H. Tan, J. Zhou, T. Wang, D. Duan, K. Fan, J. He, D. Cheng, H. Shi, H. S. Choi and X. Yan, *ACS Nano*, 2018, **12**, 9300–9308.
- 49 Z. Zhen, W. Tang, C. Guo, H. Chen and X. Lin, *ACS Nano*, 2013, **7**, 6988–6996.
- 50 P. Swietach, R. D. Vaughan-Jones, A. L. Harris and A. Hulikova, *Philos. Trans. R. Soc., B*, 2014, **369**, 20130099.
- 51 P. Arosio, R. Ingrassia and P. Cavadini, *Biochim. Biophys. Acta, Gen. Subj.*, 2009, **1790**, 589–599.
- 52 H. Alonso-Navarro, F. Javier Jimenez-Jimenez, E. Garcia-Martin and J. AG Agundez, *Curr. Drug Metab.*, 2014, **15**, 129–181.
- 53 R. C. Brown, A. P. Morris and R. G. O’Neil, *Brain Res.*, 2007, **1130**, 17–30.
- 54 Y. Omidi, L. Campbell, J. Barar, D. Connell, S. Akhtar and M. Gumbleton, *Brain Res.*, 2003, **990**, 95–112.
- 55 J. Xue, Z. Zhao, L. Zhang, L. Xue, S. Shen, Y. Wen, Z. Wei, L. Wang, L. Kong, H. Sun, Q. Ping, R. Mo and C. Zhang, *Nat. Nanotechnol.*, 2017, **12**, 692–700.
- 56 W. Wan, L. Cao, L. Liu, C. Zhang, B. Kalionis, X. Tai, Y. Li and S. Xia, *J. Neurochem.*, 2015, **134**, 382–393.
- 57 C. E. Van Skike, J. B. Jahrling, A. B. Olson, N. L. Sayre, S. A. Hussong, Z. Ungvari, J. D. Lechleiter and V. Galvan, *Am. J. Physiol.: Heart Circ. Physiol.*, 2018, **314**, H693–H703.

- 58 G. Li, M. J. Simon, L. M. Cancel, Z. D. Shi, X. Ji, J. M. Tarbell, B. Morrison 3rd and B. M. Fu, *Ann. Biomed. Eng.*, 2010, **38**, 2499–2511.
- 59 M. M. Salman, G. Marsh, I. Kusters, M. Delince, G. Di Caprio, S. Upadhyayula, G. de Nola, R. Hunt, K. G. Ohashi, T. Gray, F. Shimizu, Y. Sano, T. Kanda, B. Obermeier and T. Kirchhausen, *Front. Bioeng. Biotechnol.*, 2020, **8**, 573775.
- 60 B. A. Imhof and D. Dunon, *Adv. Immunol.*, 1995, **58**, 345–416.
- 61 N. R. Wevers, D. G. Kasi, T. Gray, K. J. Wilschut, B. Smith, R. van Vught, F. Shimizu, Y. Sano, T. Kanda, G. Marsh, S. J. Trietsch, P. Vulto, H. L. Lanz and B. Obermeier, *Fluids Barriers CNS*, 2018, **15**, 23.